Astrodynamics Vol. 6, No. 3, 269–283, 2022 https://doi.org/10.1007/s42064-021-0106-0

Out-of-plane equilibrium points and invariant manifolds about an asteroid with gravitational orbit–attitude coupling perturbation

Yue Wang (✉), Ruikang Zhang

School of Astronautics, Beihang University, Beijing 102206, China

ABSTRACT

By considering the spacecraft as an extended, rigid body with a prior known attitude instead of a point mass, the *attitude-restricted orbital dynamics* can improve the precision of the classical point-mass orbital dynamics in close proximity to an asteroid, because it includes the perturbation caused by the gravitational orbit–attitude coupling of the spacecraft (GOACP). The GOACP is defined as the difference between the gravity acting on a non-spherical, extended body (the real case of a spacecraft) and the gravity acting on a point mass (the approximation of a spacecraft in classical orbital dynamics). In-plane equilibrium points that are within the principal planes of the asteroid have been investigated for the attitude-restricted orbital dynamics in previous studies, including equatorial and in-plane non-equatorial equilibrium points. In this study, out-of-plane equilibrium points outside the principal planes of the asteroid were examined. Out-of-plane equilibrium points cannot exist in the classical point-mass orbital dynamics but do exist in the attitude-restricted orbital dynamics owing to the effects of the GOACP. The previously investigated in-plane equilibrium points and the out-of-plane ones examined in this study provide a complete map of the equilibrium points in close proximity to an asteroid with the GOACP. Equatorial and in-plane non-equatorial equilibrium points have extended the longitude and latitude ranges of the classical equilibrium points without the GOACP, respectively, while the out-of-plane ones examined in the present study extend both the longitude and latitude ranges. Additionally, the invariant manifolds of out-of-plane equilibrium points were calculated, and the results indicated that the attitude of spacecraft significantly affects the invariant manifolds. In practice, these equilibrium points can provide natural hovering positions for operations in proximity to asteroids, and their invariant manifolds can be used for transfers to or from the equilibrium points.

KEYWORDS

asteroid mission
attitude-restricted orbital dynamics
gravitational orbit–attitude coupling perturbation (GOACP)
out-of-plane equilibrium points
invariant manifolds

Research Article

Received: 11 July 2020
Accepted: 5 June 2021

1 Introduction

The *attitude-restricted orbital dynamics* refers to a newly proposed orbital model for the high-precision modeling of the translational motion of spacecraft in close proximity to an asteroid [1, 2]. In contrast to the classical orbital dynamics where the spacecraft is approximated as a point mass, the spacecraft in the attitude-restricted orbital dynamics is considered as an extended, rigid body with a prior known relative attitude with respect to the asteroid. Through this improvement, the new orbital model includes the gravitational orbit–attitude coupling perturbation (GOACP), which is neglected in the classical point-mass orbital dynamics. The GOACP is defined as the difference between the gravity acting on a non-spherical, extended body (the real case of a spacecraft) and the gravity acting on a point mass (the approximation of a spacecraft in classical orbital dynamics). Therefore, the attitude-restricted orbital dynamics can improve the precision of classical point-mass orbital dynamics, particularly in the case of significant gravitational orbit–

✉ ywang@buaa.edu.cn

attitude coupling.

Usually, the orbit–attitude coupling of spacecraft is negligible in astrodynamics and space engineering. Therefore, the orbital and attitude motions of spacecraft near asteroids have been studied separately in the orbital dynamics [3–7] and attitude dynamics [8–15], respectively. However, for a large spacecraft in proximity to a small asteroid, the gravitational orbit–attitude coupling is significant owing to the large ratio of the spacecraft's characteristic dimension to the orbit radius [16, 17]. To include the orbit–attitude coupling, the six-degree of freedom (6-DOF) gravitationally coupled orbit–attitude dynamics (also called *full dynamics*), where the spacecraft is modeled as an extended, rigid body, have been proposed and studied in different types of gravity fields [18–28], as well as with the solar radiation pressure (SRP) [29, 30]. The coupled orbit–attitude dynamics has already been adopted in studies on guidance and control of operations in proximity to asteroids [31–34], and related control problems [35].

Although the gravitational orbit–attitude coupling can be included naturally in the 6-DOF coupled orbit–attitude dynamics, from the perspective of the 3-DOF orbital motion, the coupling causes an extra orbital perturbation—the GOACP—in addition to the non-spherical gravity of the asteroid, SRP, solar tide, etc. It has been shown that the ratio of the GOACP to the non-spherical gravity is on the order of $(\rho/a_{\mathrm{e}})^2$, where ρ represents the characteristic dimension of the spacecraft and a_{e} represents the mean radius of the asteroid [1]. Therefore, the GOACP must be considered for a large spacecraft. The attitude-restricted orbital dynamics were proposed for this reason, where the word "restricted" indicates that the orbital motion is treated as a restricted problem at a prior known attitude.

The traditional spacecraft dynamics, where the attitude motion is treated as a restricted problem on the predetermined orbit, and the attitude-restricted orbital dynamics, where the orbital motion is treated as a restricted problem at the predetermined attitude, are two different approximations of the 6-DOF motion of spacecraft. Because the orbital control is usually weaker than the attitude control, the natural orbital dynamics, which can be utilized for saving fuel, are more important than the natural attitude dynamics. Therefore, the attitude-restricted orbital dynamics with the GOACP are reasonable and useful from the perspective of space engineering [1].

Wang and Xu have shown that the GOACP makes the phase space of the system complex and makes equilibrium points more diverse than those in the classical point-mass orbital dynamics without GOACP [1, 2]. Two types of equatorial equilibrium points and two families of in-plane non-equatorial equilibrium points have been obtained numerically, which extend the longitude and latitude ranges of the classical equilibrium points without GOACP, respectively. In this study, on the basis of our previous results, we investigated out-of-plane equilibrium points and their invariant manifolds, which are outside the principal planes of the asteroid. These out-of-plane equilibrium points extend the longitude and latitude ranges of classical equilibrium points simultaneously. Compared with our previous results, this study provides more details on the phase space of the system, as well as more natural hovering positions and transfer trajectories for asteroid missions.

The remainder of this paper is organized as follows. The equations of motion are presented in Section 2, followed by the equilibrium conditions in Section 3. Out-of-plane equilibrium points are calculated in Section 4, and their invariant manifolds are analyzed in Section 5. Finally, the paper is concluded in Section 6.

2 Equations of motion

The system studied by Wang and Xu is examined here [1, 2]. As shown in Fig. 1, the principal-axis body-fixed reference frames of the asteroid and spacecraft are given by $S_{\mathrm{P}} = \{\boldsymbol{u}, \boldsymbol{v}, \boldsymbol{w}\}$ and $S_{\mathrm{B}} = \{\boldsymbol{i}, \boldsymbol{j}, \boldsymbol{k}\}$, respectively. The asteroid rotates uniformly at a constant angular velocity

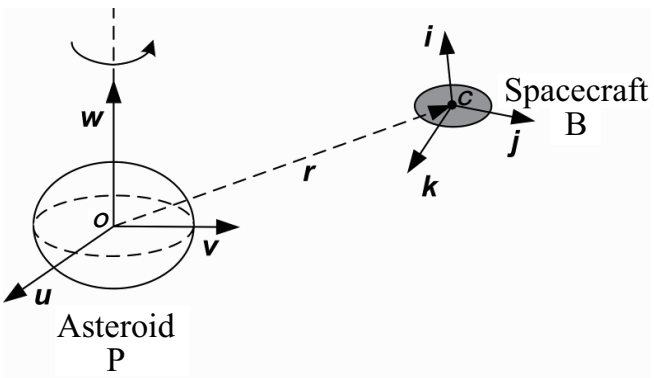

Fig. 1 Spacecraft moving in close proximity to a small asteroid.

ω_T, and its non-spherical gravity field is described by the harmonic coefficients C_{20} and C_{22}. The relative attitude of the spacecraft with respect to the asteroid is described by $\boldsymbol{A}$:

$$\boldsymbol{A} = [\boldsymbol{\alpha}, \boldsymbol{\beta}, \boldsymbol{\gamma}]^{\mathrm{T}} \in SO(3) \tag{1}$$

where $\boldsymbol{\alpha}$, $\boldsymbol{\beta}$, and $\boldsymbol{\gamma}$ represent the coordinates of $\boldsymbol{u}$, $\boldsymbol{v}$, and $\boldsymbol{w}$ in the body-fixed frame of the spacecraft S_{B}, respectively. $\boldsymbol{r} = [x, y, z]^{\mathrm{T}}$ represents the position of the spacecraft in the body-fixed frame of the asteroid S_{P} with the unit vector $\bar{\boldsymbol{r}} = [\bar{x}, \bar{y}, \bar{z}]^{\mathrm{T}}$ along it. m and $\boldsymbol{I} = \mathrm{diag}\{I_{xx}, I_{yy}, I_{zz}\}$ represent the mass and inertia tensor of the spacecraft, respectively.

The equations of orbital motion of the spacecraft expressed in the body-fixed frame of the asteroid S_{P} are given by

$$\ddot{\boldsymbol{r}} + 2\boldsymbol{\omega}_T \times \dot{\boldsymbol{r}} + \boldsymbol{\omega}_T \times (\boldsymbol{\omega}_T \times \boldsymbol{r}) = \boldsymbol{\alpha}_{\mathrm{s/c}} \tag{2}$$

where $\boldsymbol{\alpha}_{\mathrm{s/c}}$ represents the acceleration acting on the spacecraft and $\boldsymbol{\omega}_T = [0, 0, \omega_T]^{\mathrm{T}}$.

In the attitude-restricted orbital dynamics, the non-spherical gravity perturbation of the asteroid and the GOACP are considered, while the perturbations of the SRP and solar tide are neglected [1]. Accordingly, the acceleration $\boldsymbol{\alpha}_{\mathrm{s/c}}$ is given as

$$\boldsymbol{\alpha}_{\mathrm{s/c}} = \boldsymbol{\alpha}_{\mathrm{Kepler}} + \boldsymbol{\alpha}_{\mathrm{NSG}} + \boldsymbol{\alpha}_{\mathrm{OAC}} \tag{3}$$

where $\boldsymbol{\alpha}_{\mathrm{Kepler}}$ represents the Kepler two-body acceleration.

$$\boldsymbol{\alpha}_{\mathrm{Kepler}} = -\frac{\mu}{r^2}\bar{\boldsymbol{r}} \tag{4}$$

Here, $\mu = GM$, M represents the mass of the asteroid, and G is the gravitational constant. $\boldsymbol{\alpha}_{\mathrm{NSG}}$ represents the non-spherical gravity perturbation of the asteroid up to the second order:

$$\begin{aligned}\boldsymbol{\alpha}_{\mathrm{NSG}} = \frac{3\mu}{2r^4}\{&[\tau_0(1-5\bar{z}^2) - 10\tau_2(\bar{x}^2 - \bar{y}^2)]\bar{\boldsymbol{r}} \\ &+ 2\tau_0\bar{z}\boldsymbol{e}_3 + 4\tau_2(\bar{x}\boldsymbol{e}_1 - \bar{y}\boldsymbol{e}_2)\}\end{aligned} \tag{5}$$

where $\tau_0 = a_{\mathrm{e}}^2 C_{20}$, $\tau_2 = a_{\mathrm{e}}^2 C_{22}$, a_{e} represents the mean equatorial radius of the asteroid, $\boldsymbol{e}_1 = [1, 0, 0]^{\mathrm{T}}$, $\boldsymbol{e}_2 = [0, 1, 0]^{\mathrm{T}}$, and $\boldsymbol{e}_3 = [0, 0, 1]^{\mathrm{T}}$. $\boldsymbol{\alpha}_{\mathrm{OAC}}$ represents the GOACP up to the second order:

$$\begin{aligned}\boldsymbol{\alpha}_{\mathrm{OAC}} = \frac{3\mu}{2r^4}\Bigg\{&\left[5\bar{\boldsymbol{r}}^{\mathrm{T}}\boldsymbol{A}\left(\frac{\boldsymbol{I}}{m}\right)\boldsymbol{A}^{\mathrm{T}}\bar{\boldsymbol{r}} - \mathrm{tr}\left(\frac{\boldsymbol{I}}{m}\right)\right]\bar{\boldsymbol{r}} \\ &- 2\boldsymbol{A}\left(\frac{\boldsymbol{I}}{m}\right)\boldsymbol{A}^{\mathrm{T}}\bar{\boldsymbol{r}}\Bigg\}\end{aligned} \tag{6}$$

In the gravitational acceleration $\boldsymbol{\alpha}_{\mathrm{s/c}}$, $\boldsymbol{\alpha}_{\mathrm{Kepler}}$ is the zeroth-order term, and $\boldsymbol{\alpha}_{\mathrm{NSG}}$ and $\boldsymbol{\alpha}_{\mathrm{OAC}}$ are the second-order terms [1].

From the perspective of rigid-body dynamics, the spacecraft's parameter $\boldsymbol{I}/m$ is essential for the GOACP $\boldsymbol{\alpha}_{\mathrm{OAC}}$, because $\boldsymbol{I}/m$ determines the difference between the spacecraft and a point mass (or a homogenous sphere). $\boldsymbol{I}/m$ is determined by the mass distribution parameters σ_x and σ_y, as well as the characteristic dimension ρ of the spacecraft, which are defined as Eq. (7) [26]:

$$\sigma_x = (I_{zz} - I_{yy})/I_{xx}, \sigma_y = (I_{zz} - I_{xx})/I_{yy}, \rho^2 = 2I_{xx}/m \tag{7}$$

The GOACP $\boldsymbol{\alpha}_{\mathrm{OAC}}$ is more significant in the case of a more non-spherical mass distribution or a larger ratio ρ/r.

3 Equilibrium condition

At the equilibrium points, the spacecraft remains stationary in the body-fixed frame of the asteroid. The equilibrium condition can be obtained by simply letting $\ddot{\boldsymbol{r}} = \boldsymbol{0}$ and $\dot{\boldsymbol{r}} = \boldsymbol{0}$ in equation of motion (2):

$$\boldsymbol{\omega}_T \times (\boldsymbol{\omega}_T \times \boldsymbol{r}) = \boldsymbol{\alpha}_{\mathrm{s/c}} \tag{8}$$

Thus, the gravitational force $\boldsymbol{\alpha}_{\mathrm{s/c}}$ balances the centrifugal force of the orbital motion. By using Eqs. (3)–(6), the equilibrium condition (8) can be written as

$$\begin{aligned}&\boldsymbol{\omega}_T \times (\boldsymbol{\omega}_T \times \boldsymbol{r}) = \\ &\quad -\frac{\mu}{r^2}\bar{\boldsymbol{r}} + \frac{3\mu}{2r^4}\{[\tau_0(1-5\bar{z}^2) - 10\tau_2(\bar{x}^2 - \bar{y}^2)]\bar{\boldsymbol{r}} \\ &\quad + 2\tau_0\bar{z}\boldsymbol{e}_3 + 4\tau_2(\bar{x}\boldsymbol{e}_1 - \bar{y}\boldsymbol{e}_2)\} \\ &\quad + \frac{3\mu}{2r^4}\Bigg\{\left[5\bar{\boldsymbol{r}}^{\mathrm{T}}\boldsymbol{A}\left(\frac{\boldsymbol{I}}{m}\right)\boldsymbol{A}^{\mathrm{T}}\bar{\boldsymbol{r}} - \mathrm{tr}\left(\frac{\boldsymbol{I}}{m}\right)\right]\bar{\boldsymbol{r}} \\ &\quad - 2\boldsymbol{A}\left(\frac{\boldsymbol{I}}{m}\right)\boldsymbol{A}^{\mathrm{T}}\bar{\boldsymbol{r}}\Bigg\}\end{aligned} \tag{9}$$

3.1 Classical results without GOACP

Howard studied the equilibrium points of the classical point-mass orbital dynamics in proximity to an asteroid [36]. Without the GOACP, the acceleration of the spacecraft is given by $\boldsymbol{\alpha}_{\mathrm{s/c}} = \boldsymbol{\alpha}_{\mathrm{Kepler}} + \boldsymbol{\alpha}_{\mathrm{NSG}}$. Thus, the equilibrium condition is

$$\begin{aligned}\boldsymbol{\omega}_T \times (\boldsymbol{\omega}_T \times \boldsymbol{r}) = -\frac{\mu}{r^2}\bar{\boldsymbol{r}} + \frac{3\mu}{2r^4}\{&[\tau_0(1-5\bar{z}^2) \\ &- 10\tau_2(\bar{x}^2 - \bar{y}^2)]\bar{\boldsymbol{r}} + 2\tau_0\bar{z}\boldsymbol{e}_3 + 4\tau_2(\bar{x}\boldsymbol{e}_1 - \bar{y}\boldsymbol{e}_2)\}\end{aligned} \tag{10}$$

Using Eq. (10), Howard determined the in-plane equilibrium points that are within the principal planes of the asteroid, including the equatorial and in-plane non-equatorial equilibrium points [36]. However, by performing simple analyses, we found that out-of-plane equilibrium points that are outside principal planes of the asteroid cannot exist in the classical point-mass orbital

dynamics. All the terms in Eq. (10) except $4\tau_2(\bar{x}\boldsymbol{e}_1 - \bar{y}\boldsymbol{e}_2)$ are naturally within the plane spanned by $\boldsymbol{\omega}_T$ and $\boldsymbol{r}$. Thus, Eq. (10) requires that $4\tau_2(\bar{x}\boldsymbol{e}_1 - \bar{y}\boldsymbol{e}_2)$ is also within the plane spanned by $\boldsymbol{\omega}_T$ and $\boldsymbol{r}$, that is, parallel to $\bar{x}\boldsymbol{e}_1 + \bar{y}\boldsymbol{e}_2$, implying that $\bar{x} = 0$ or $\bar{y} = 0$. Therefore, the equilibrium points must be within the principal planes of the asteroid and cannot be out-of-plane ones.

3.2 Equilibrium condition with GOACP

Owing to the GOACP $\boldsymbol{\alpha}_{\mathrm{OAC}}$, out-of-plane equilibrium points may exist in the attitude-restricted orbital dynamics. For out-of-plane equilibrium points, we have $\bar{x}\bar{y}\bar{z} \neq 0$; the equilibrium condition (9) cannot be simplified further. In contrast to the in-plane equilibrium points reported by Wang and Xu [1, 2], there is not a specific geometric relationship between principal planes of the asteroid and the spacecraft. Thus, for out-of-plane equilibrium points, three Euler angles are needed to describe the relative attitude of the spacecraft with respect to the asteroid, making it tedious to determine the equilibrium condition.

The sequence of rotation from the frame S_{P} to the spacecraft body-fixed frame S_{B} is as follows: the yaw angle ψ around $\boldsymbol{k}$-axis, the pitch angle θ around $\boldsymbol{j}$-axis, and the roll angle ϕ around the $\boldsymbol{i}$-axis. Then, the relative attitude matrix $\boldsymbol{A}$, which is also the coordinate transformation matrix from frame S_{B} to frame S_{P}, is given by

$$\begin{aligned}\boldsymbol{A} &= [\boldsymbol{\alpha}, \boldsymbol{\beta}, \boldsymbol{\gamma}]^{\mathrm{T}} \\ &= \begin{bmatrix} \cos\psi & -\sin\psi & 0 \\ \sin\psi & \cos\psi & 0 \\ 0 & 0 & 1 \end{bmatrix} \cdot \begin{bmatrix} \cos\theta & 0 & \sin\theta \\ 0 & 1 & 0 \\ -\sin\theta & 0 & \cos\theta \end{bmatrix} \\ &\quad \cdot \begin{bmatrix} 1 & 0 & 0 \\ 0 & \cos\phi & -\sin\phi \\ 0 & \sin\phi & \cos\phi \end{bmatrix} \end{aligned} \tag{11}$$

The equilibrium condition (9) can be rewritten as

$$\begin{aligned}\boldsymbol{\omega}_T \times (\boldsymbol{\omega}_T \times \boldsymbol{r}) = &-\frac{\mu}{r^2}\bar{\boldsymbol{r}} + \frac{3\mu}{2r^4}\Bigg[\tau_0(1 - 5\bar{z}^2) \\ &- 10\tau_2(\bar{x}^2 - \bar{y}^2) + 5\bar{\boldsymbol{r}}^{\mathrm{T}}\boldsymbol{A}\left(\frac{\boldsymbol{I}}{m}\right)\boldsymbol{A}^{\mathrm{T}}\bar{\boldsymbol{r}} - \mathrm{tr}\left(\frac{\boldsymbol{I}}{m}\right)\Bigg]\bar{\boldsymbol{r}} \\ &+ \frac{3\mu}{r^4}\left[\tau_0\bar{z}\boldsymbol{e}_3 + 2\tau_2(\bar{x}\boldsymbol{e}_1 - \bar{y}\boldsymbol{e}_2) - \boldsymbol{A}\left(\frac{\boldsymbol{I}}{m}\right)\boldsymbol{A}^{\mathrm{T}}\bar{\boldsymbol{r}}\right]\end{aligned} \tag{12}$$

4 Out-of-plane equilibrium points

In this section, we present calculation examples for the out-of-plane equilibrium points and investigate the effects of the GOACP $\boldsymbol{\alpha}_{\mathrm{OAC}}$ on their distributions. The parameters of the asteroid are identical to those of the example asteroid considered by Wang and Xu [1, 2]:

$$\begin{cases} \mu = 5\ \mathrm{m}^3/\mathrm{s}^2,\ C_{20} = -0.12,\ C_{22} = 0.01 \\ a_{\mathrm{e}} = 250\ \mathrm{m},\ \omega_T = 2.9089 \times 10^{-4}\ \mathrm{s}^{-1} \end{cases} \tag{13}$$

The mass distribution of the spacecraft is identical to that used by Wang and Xu [2]:

$$I_{xx} : I_{yy} : I_{zz} = 1.5 : 1.2 : 1 \tag{14}$$

To show the effects of the GOACP, three large values are chosen for the characteristic dimension of the spacecraft ρ:

$$\rho = 50\ \mathrm{m}, \quad \rho = 100\ \mathrm{m}, \quad \rho = 160\ \mathrm{m} \tag{15}$$

which represent larger spacecraft in future asteroid missions, e.g., the asteroid deflection mission and asteroid resource exploitation.

We calculate the out-of-plane equilibrium points by solving equilibrium condition (12) via a numerical method. The *fsolve* function in the software MATLAB is used, which relies on an iteration procedure and requires an initial guess.

The in-plane equilibrium points obtained in previous studies can be adopted as starting points of the iterations. With in-plane equilibrium points with a single nonzero Euler angle ψ, θ, or ϕ obtained by Wang and Xu [1, 2], we can calculate the out-of-plane equilibrium points when the other two Euler angles, i.e., (θ, ϕ), (ψ, ϕ), or (ψ, θ) increase gradually with small step sizes. The equilibrium points corresponding to the last set of Euler angles can be used as the initial guesses for the current set of Euler angles. The considered ranges of all the Euler angles are $[0, \pi]$, because $[\pi, 2\pi]$ is identical to $[0, \pi]$ owing to the symmetry of the spacecraft's inertia tensor. Thus, we can obtain the distributions of out-of-plane equilibrium points with different sets of Euler angles (ψ, θ, ϕ).

Two types of starting points can be used for the iterations during the calculation of out-of-plane equilibrium points: the equatorial equilibrium points with nonzero Euler angle ψ [1] and the in-plane non-equatorial equilibrium points with a nonzero Euler angle θ or nonzero Euler angle ϕ [2]. Among the two families of in-plane non-equatorial equilibrium points obtained by Wang and Xu [2], we only consider the out-of-plane equilibrium points near the first family that is near the equatorial principal axes of the asteroid, because

the second family, which can exist only in the case of a fictitious asteroid rotating around its intermediate-moment principal axis, has limited practical significance.

4.1 To start with in-plane equilibrium points

The in-plane equilibrium points with the single nonzero Euler angle [1, 2], including the equatorial equilibrium points with nonzero Euler angle ψ [1] and the first family of the in-plane non-equatorial equilibrium points with nonzero Euler angle θ or ϕ [2], are shown in Figs. 2–4 with three values of the characteristic dimension ρ, respectively. The values of the nonzero Euler angle at the equilibrium points are indicated by their colors. Because the distributions of the equilibrium points are symmetric with respect to the center of the asteroid, only two regions are magnified in the figures.

The equatorial equilibrium points with nonzero Euler angle ψ obtained by Wang and Xu [1] are represented by the larger closed curves within the equatorial plane. The first family of in-plane non-equatorial equilibrium points with nonzero Euler angle θ or ϕ obtained by Wang and Xu [2] are represented by the smaller closed curves within the longitudinal principal plane, $\boldsymbol{u}$–$\boldsymbol{w}$ plane, and $\boldsymbol{v}$–$\boldsymbol{w}$ plane, respectively. We see that the curves of equatorial equilibrium points intersect with those of in-plane non-equatorial equilibrium points at the points with three zero Euler angles. In the following, the equatorial equilibrium points with nonzero Euler angle ψ obtained by Wang and Xu [1] are needed as starting points for the iterations during the calculation of out-of-plane equilibrium points.

4.2 Out-of-plane equilibrium points with nonzero ψ and ϕ

Choosing the equatorial equilibrium points with nonzero Euler angle ψ [1] as starting points for the iterations, we first calculate the out-of-plane equilibrium points with $\{\psi \in [0, \pi], \theta = 0, \phi \in [0, \pi]\}$ for three values of the characteristic dimension ρ.

For each value of ρ, the details of the process are as follows. First, a series of equatorial equilibrium points with a grid size of 3 degrees for ψ, i.e., the equatorial equilibrium points with $\{\psi = 3i\,\mathrm{deg}, \theta = \phi = 0\}$, $i = \{0, 1, \cdots, 59\}$, are selected. Then, with every equatorial equilibrium point with $\{\psi = 3i\,\mathrm{deg}, \theta = \phi = 0\}$, $i \in \{0, 1, \cdots, 59\}$ as the starting point, out-of-plane equilibrium points with $\{\psi = 3i\,\mathrm{deg}, \theta = 0, \phi \in [0, \pi]\}$, $i \in \{0, 1, \cdots, 59\}$ are calculated as the Euler angle ϕ increases gradually from 0 to π with a small step size via iteration processes. Finally, by plotting all the out-of-plane equilibrium points with $\{\psi = 3i\,\mathrm{deg}, \theta = 0, \phi \in [0, \pi]\}$, $i \in \{0, 1, \cdots, 59\}$, the loci of out-of-plane equilibrium points with $\{\psi \in [0, \pi], \theta = 0, \phi \in [0, \pi]\}$ are obtained for the three values of the characteristic dimension ρ, as shown in Figs. 5–7, respectively. Because the distributions of the equilibrium points are symmetric with respect to the center of the

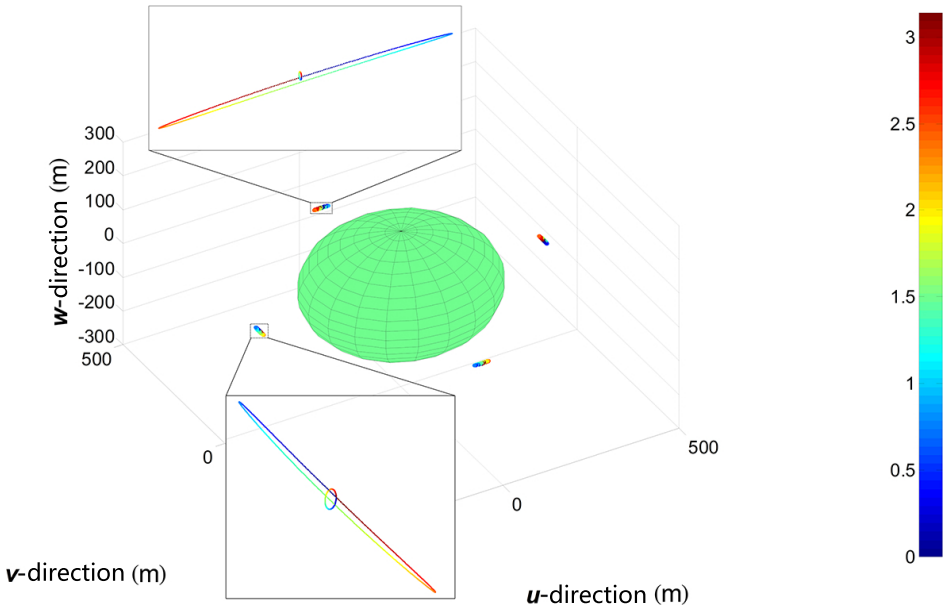

Fig. 2 Loci of in-plane equilibrium points with a single nonzero Euler angle and $\rho = 50$ m.

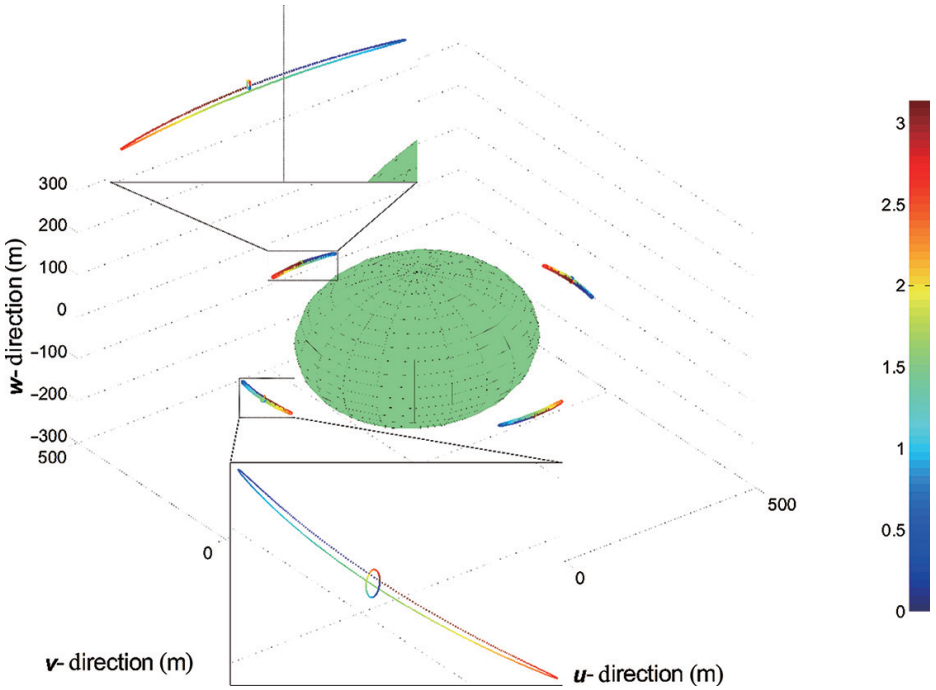

Fig. 3 Loci of in-plane equilibrium points with a single nonzero Euler angle and $\rho = 100$ m.

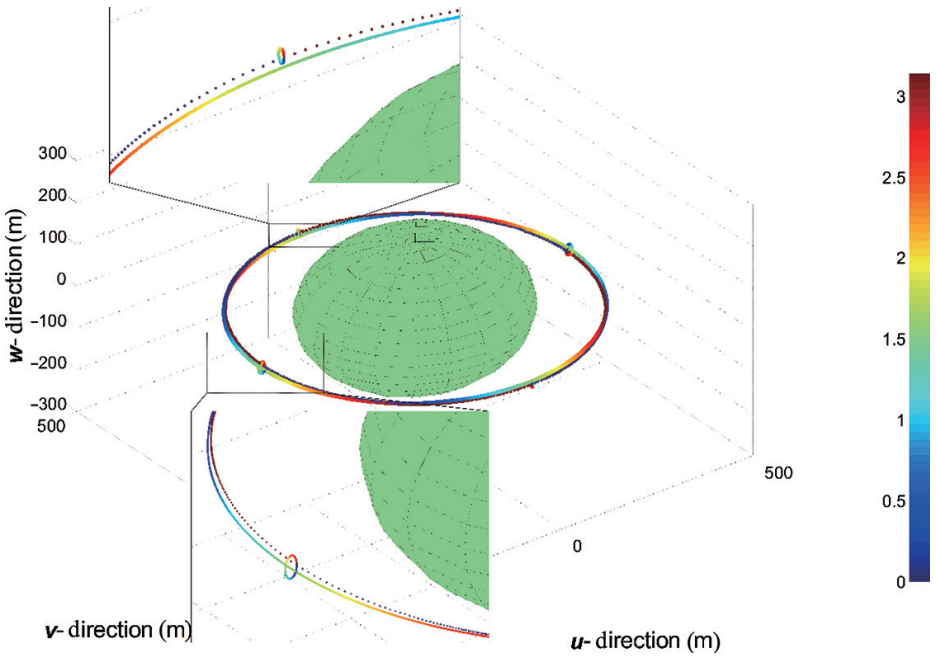

Fig. 4 Loci of in-plane equilibrium points with a single nonzero Euler angle and $\rho = 160$ m.

asteroid, only two regions are magnified in the figures.

Each group of out-of-plane equilibrium points with $\{\psi = 3i\,\text{deg}, \theta = 0, \phi \in [0, \pi]\}$, which are calculated via iterations starting from the same equatorial equilibrium point with $\{\psi = 3i\,\text{deg}, \theta = \phi = 0\}$, forms a closed curve. Therefore, the loci of the out-of-plane equilibrium points with $\{\psi \in [0, \pi], \theta = 0, \phi \in [0, \pi]\}$ form a two-dimensional (2D) surface consisting of infinitely many closed curves, each of which is formed by out-of-plane equilibrium points with $\{\psi = \psi_{\text{curve}}, \theta = 0, \phi \in [0, \pi]\}$. ψ_{curve} is the value of the Euler angle ψ for the closed curve and is the value of ψ for the closed curve's starting point. Thus, the 2D surface

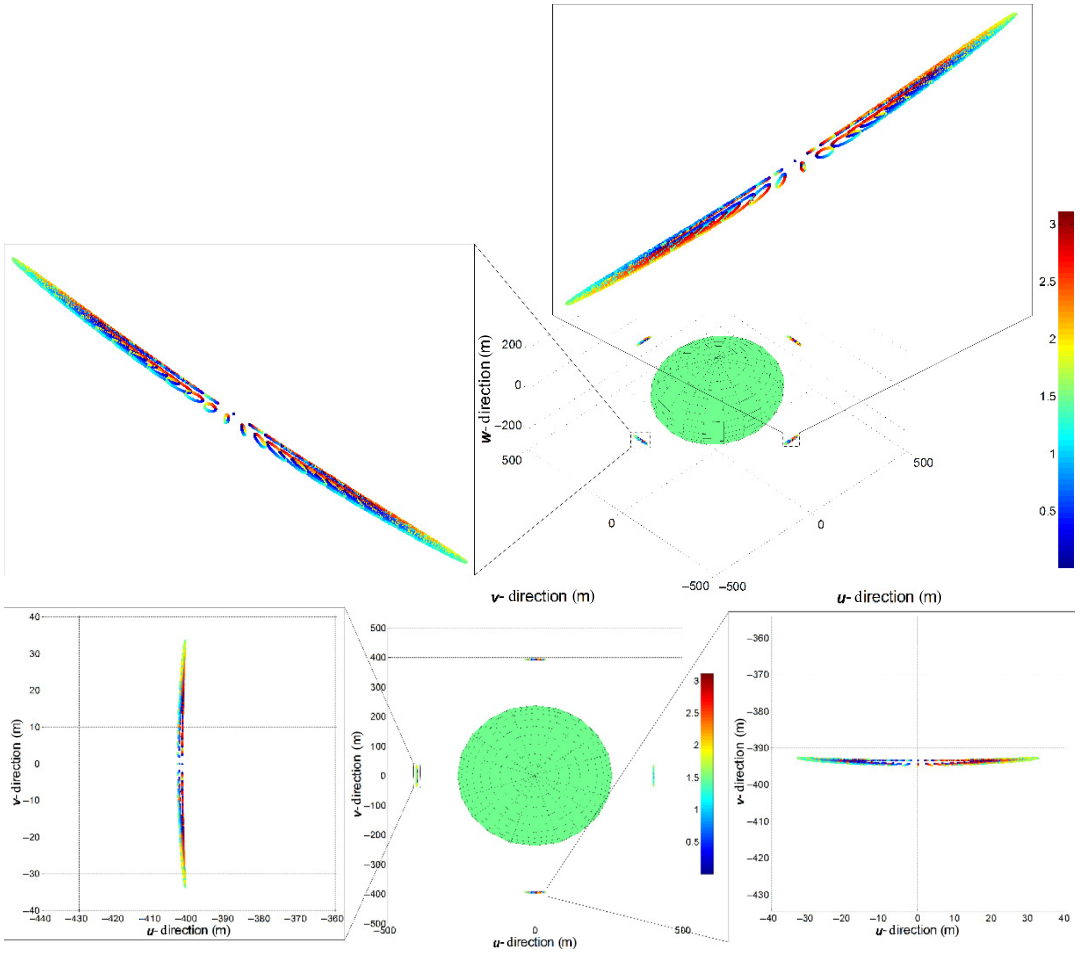

Fig. 5 Loci of out-of-plane equilibrium points with $\{\psi \in [0, \pi], \theta = 0, \phi \in [0, \pi]\}$ and $\rho = 50$ m.

of out-of-plane equilibrium points can be parameterized by the pair of Euler angles $\{\psi, \phi\}$. In the figures, the values of the Euler angle ϕ at the equilibrium points are represented by different colors.

Generally, the 2D surface surrounds the in-plane equatorial equilibrium points, which can be regarded as its framework. For a small characteristic dimension ρ, the 2D surface is distributed near the equatorial axes of the asteroid, as shown in Figs. 5 and 6, whereas for a large characteristic dimension ρ, the 2D surface can be distributed around the asteroid at any longitude owing to the significant GOACP, as shown in Fig. 7.

As mentioned previously, the second family of in-plane non-equatorial equilibrium points with the nonzero Euler angle θ or ϕ reported by Wang and Xu [2] can be calculated together with the out-of-plane equilibrium points. As expected, the second family of in-plane non-equatorial equilibrium points with nonzero Euler angle θ or ϕ can be identified in Figs. 5–7 as the two closed curves near the $\boldsymbol{v}$-axis with $\{\psi = 0, \theta = 0, \phi \in [0, \pi]\}$ and the other two closed curves near the $\boldsymbol{u}$-axis with $\{\psi = 90\,\text{deg}, \theta = 0, \phi \in [0, \pi]\}$.

Importantly, the two closed curves near the $\boldsymbol{u}$-axis with $\{\psi = 0, \theta = 0, \phi \in [0, \pi]\}$ and the other two closed curves near the $\boldsymbol{v}$-axis with $\{\psi = 90\,\text{deg}, \theta = 0, \phi \in [0, \pi]\}$ degenerate into four points, as shown in the figures. This is because in these cases, the rotational axis of ϕ—the $\boldsymbol{i}$-axis of the spacecraft—is parallel to the $\boldsymbol{u}$-axis or $\boldsymbol{v}$-axis of the asteroid, on which the starting points of the closed curves are located, and the Euler angle ϕ only affects higher-order terms of the gravitational force, having no influence on the locations of the equilibrium points, as reported by Wang and Xu [1].

4.3 Out-of-plane equilibrium points with nonzero ψ and θ

By using a process similar to that described in Section 4.2,

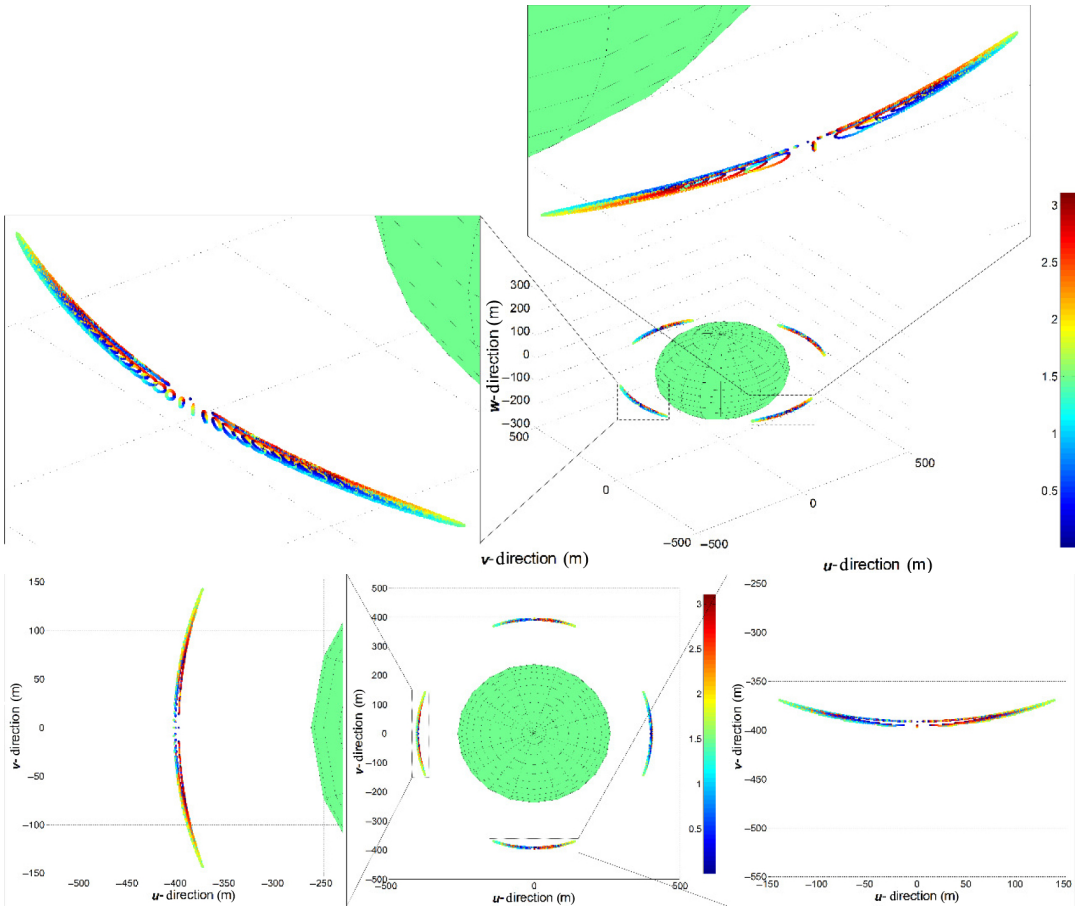

Fig. 6 Loci of out-of-plane equilibrium points with $\{\psi \in [0,\pi], \theta = 0, \phi \in [0,\pi]\}$ and $\rho = 100$ m.

we can calculate the out-of-plane equilibrium points with $\{\psi \in [0,\pi], \theta \in [0,\pi], \phi = 0\}$ for the three values of the characteristic dimension ρ. First, the same equatorial equilibrium points with $\{\psi = 3i\,\mathrm{deg}, \theta = \phi = 0\}$, $i = \{0, 1, \cdots, 59\}$ selected in Section 4.2 are chosen. Then, with every equatorial equilibrium point with $\{\psi = 3i\,\mathrm{deg}, \theta = \phi = 0\}$, $i \in \{0, 1, \cdots, 59\}$ as the starting point, out-of-plane equilibrium points with $\{\psi = 3i\,\mathrm{deg}, \theta \in [0,\pi], \phi = 0\}$, $i \in \{0, 1, \cdots, 59\}$ are calculated as the Euler angle θ increases gradually from 0 to π with a small step size via iteration processes. Finally, the loci of the out-of-plane equilibrium points with $\{\psi \in [0,\pi], \theta \in [0,\pi], \phi = 0\}$ are obtained, as shown in Figs. 8–10, for the three values of the characteristic dimension ρ, respectively.

Similar to the results obtained in Section 4.2, each group of out-of-plane equilibrium points with $\{\psi = 3i\,\mathrm{deg}, \theta \in [0,\pi], \phi = 0\}$, which are calculated via iterations starting from the same equatorial equilibrium point with $\{\psi = 3i\,\mathrm{deg}, \theta = \phi = 0\}$, forms a closed curve. In contrast to the results obtained in Section 4.2, the closed curves overlap, making them difficult to distinguish. Nonetheless, the basic properties are revealed in the figures.

The loci of the out-of-plane equilibrium points with $\{\psi \in [0,\pi], \theta \in [0,\pi], \phi = 0\}$ form a 2D surface consisting of infinitely many closed curves, each of which is formed by out-of-plane equilibrium points with $\{\psi = \psi_{\mathrm{curve}}, \theta \in [0,\pi], \phi = 0\}$, where ψ_{curve} represents the Euler angle ψ for the closed curve. The 2D surface of out-of-plane equilibrium points can be parameterized by the pair of Euler angles $\{\psi, \theta\}$. In the figures, the values of the Euler angle θ are represented by different colors.

Similar to the case of Section 4.2, the 2D surface surrounds the in-plane equatorial equilibrium points, which can be regarded as its framework. For a small characteristic dimension ρ, the 2D surface is distributed near the equatorial axes of the asteroid, whereas for a large characteristic dimension ρ, the 2D surface can be distributed around the asteroid at any longitude, as

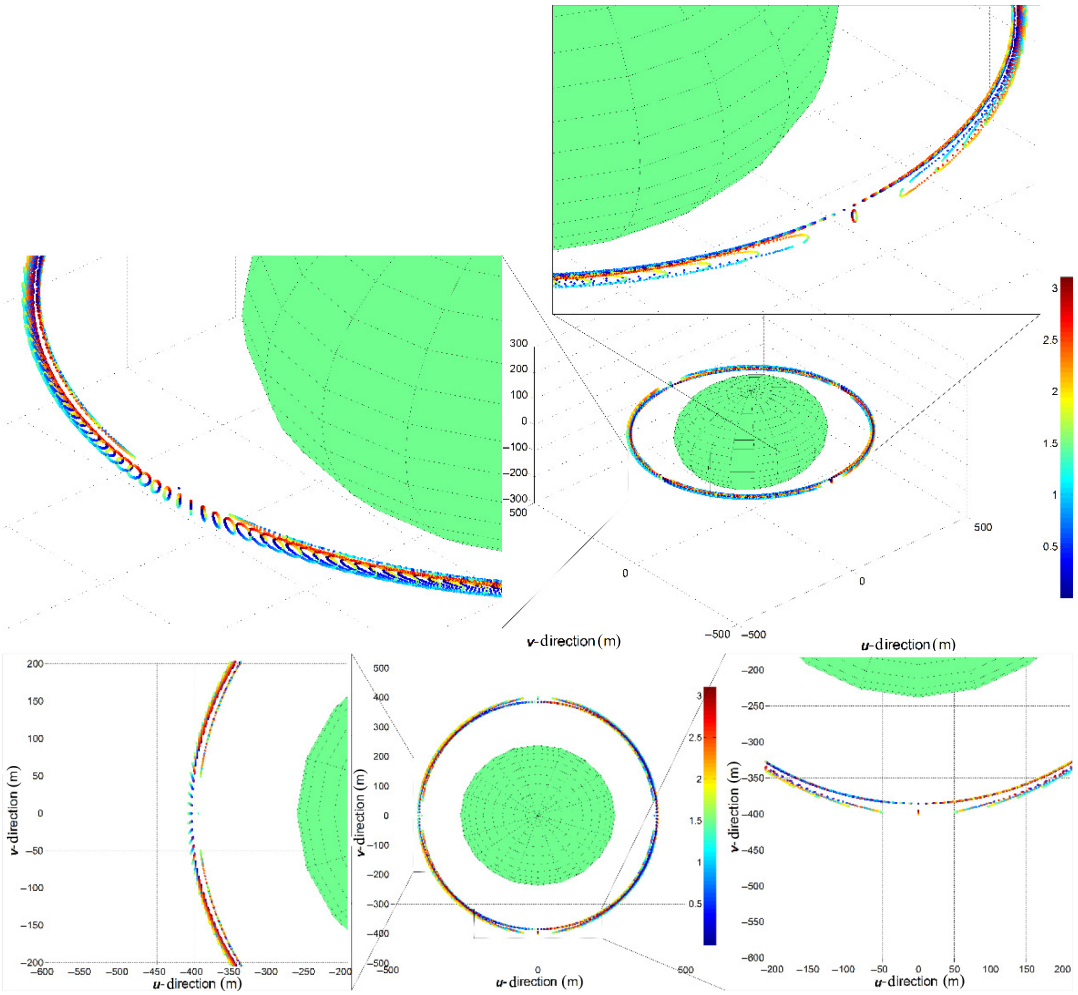

Fig. 7 Loci of out-of-plane equilibrium points with $\{\psi \in [0, \pi], \theta = 0, \phi \in [0, \pi]\}$ and $\rho = 160$ m.

shown in Fig. 10.

The second family of in-plane non-equatorial equilibrium points with nonzero Euler angle θ or ϕ can be identified in Figs. 8–10 as the two closed curves near the $\boldsymbol{u}$-axis with $\{\psi = 0, \theta \in [0, \pi], \phi = 0\}$ and the other two closed curves near the $\boldsymbol{v}$-axis with $\{\psi = 90\,\text{deg}, \theta \in [0, \pi], \phi = 0\}$. The two closed curves near the $\boldsymbol{v}$-axis with $\{\psi = 0, \theta \in [0, \pi], \phi = 0\}$ and the other two closed curves near the $\boldsymbol{u}$-axis with $\{\psi = 90\,\text{deg}, \theta \in [0, \pi], \phi = 0\}$ degenerate into four points, for the same reason mentioned in Section 4.2. Clearly, these phenomena are dual to those in Section 4.2.

The out-of-plane equilibrium points with three nonzero Euler angles, i.e., with $\{\psi \in [0, \pi], \theta \in [0, \pi], \phi \in [0, \pi]\}$, can be calculated by using the same method, but the computational burden is large, and the results are difficult to display. Thus, we do not calculate them here. It is expected that the loci of out-of-plane equilibrium points with $\{\psi \in [0, \pi], \theta \in [0, \pi], \phi \in [0, \pi]\}$ form a three-dimensional (3D) geometric object consisting of infinitely many 2D surfaces and can be parameterized by the three Euler angles $\{\psi, \theta, \phi\}$.

5 Invariant manifolds of equilibrium points with GOACP

Invariant manifolds are important dynamical structures of equilibrium points and are useful for spacecraft trajectory design. Similar to the equilibrium points, the invariant manifolds with GOACP are distinct from those of classical equilibrium points without GOACP. In this subsection, we present calculation examples of invariant manifolds and show their dependences on the spacecraft attitude.

To calculate the invariant manifolds of equilibrium points, we start with the linearized equations of motion

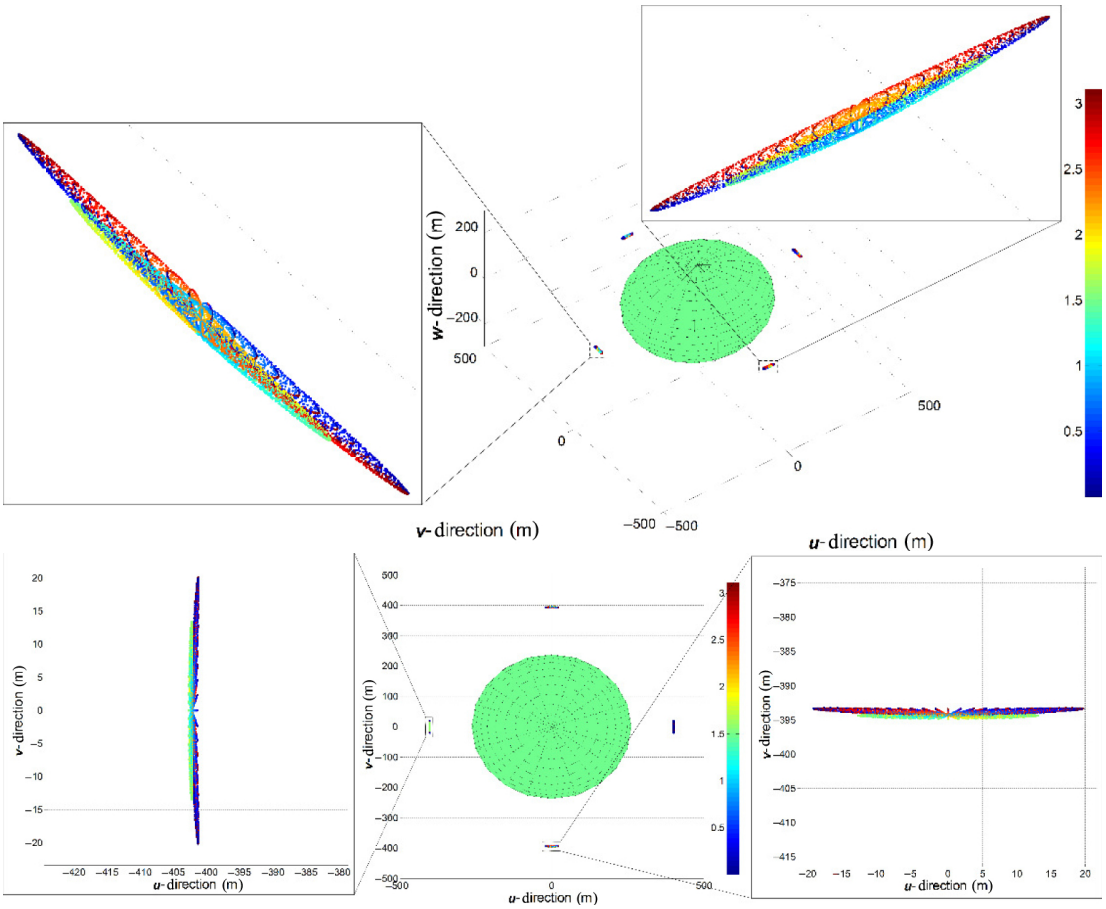

Fig. 8 Loci of out-of-plane equilibrium points with $\{\psi \in [0,\pi], \theta \in [0,\pi], \phi = 0\}$ and $\rho = 50$ m.

near the equilibrium point $\boldsymbol{r}_{\mathrm{e}}$. According to Wang and Xu [1], the linearized equation near $\boldsymbol{r}_{\mathrm{e}}$ is given by

$$\frac{\mathrm{d}}{\mathrm{d}t}\begin{bmatrix}\delta\boldsymbol{r}\\ \delta\dot{\boldsymbol{r}}\end{bmatrix} = \begin{bmatrix}\boldsymbol{0} & \boldsymbol{E}\\ -\omega_T^2\hat{\boldsymbol{e}}_3\hat{\boldsymbol{e}}_3 + \left.\frac{\partial\boldsymbol{\alpha}_{\mathrm{s/c}}}{\partial\boldsymbol{r}}\right|_{\mathrm{e}} & -2\omega_T\hat{\boldsymbol{e}}_3\end{bmatrix}\begin{bmatrix}\delta\boldsymbol{r}\\ \delta\dot{\boldsymbol{r}}\end{bmatrix} \tag{16}$$

where $\boldsymbol{E}$ represents the 3×3 identity matrix, and the hat map "$\hat{}$" is

$$\hat{\boldsymbol{e}}_3 = \begin{bmatrix}0 & -1 & 0\\ 1 & 0 & 0\\ 0 & 0 & 0\end{bmatrix} \tag{17}$$

The dynamics of the linearized system is determined by the system matrix at $\boldsymbol{r}_{\mathrm{e}}$:

$$\boldsymbol{D}(\boldsymbol{r}_{\mathrm{e}}) = \begin{bmatrix}\boldsymbol{0} & \boldsymbol{E}\\ -\omega_T^2\hat{\boldsymbol{e}}_3\hat{\boldsymbol{e}}_3 + \left.\frac{\partial\boldsymbol{\alpha}_{\mathrm{s/c}}}{\partial\boldsymbol{r}}\right|_{\mathrm{e}} & -2\omega_T\hat{\boldsymbol{e}}_3\end{bmatrix} \tag{18}$$

where the gradient of $\alpha_{\mathrm{s/c}}$ is given by

$$\begin{aligned}\frac{\partial\boldsymbol{\alpha}_{\mathrm{s/c}}}{\partial\boldsymbol{r}} = &-\frac{\mu}{r^3}(\boldsymbol{E} - 3\bar{\boldsymbol{r}}\bar{\boldsymbol{r}}^{\mathrm{T}})\\ &-\frac{3\mu}{2r^5}\left[5\bar{\boldsymbol{r}}^{\mathrm{T}}\boldsymbol{A}\left(\frac{\boldsymbol{I}}{m}\right)\boldsymbol{A}^{\mathrm{T}}\bar{\boldsymbol{r}} - \mathrm{tr}\left(\frac{\boldsymbol{I}}{m}\right)\right.\\ &\left.+\tau_0(1-5\bar{z}^2) - 10\tau_2(\bar{x}^2-\bar{y}^2)\right](7\bar{\boldsymbol{r}}\bar{\boldsymbol{r}}^{\mathrm{T}} - \boldsymbol{E})\\ &-\frac{3\mu}{r^5}\left\{\left[\mathrm{tr}\left(\frac{\boldsymbol{I}}{m}\right) - \tau_0\right]\bar{\boldsymbol{r}}\bar{\boldsymbol{r}}^{\mathrm{T}} + \boldsymbol{A}\left(\frac{\boldsymbol{I}}{m}\right)\boldsymbol{A}^{\mathrm{T}}\right.\\ &\left.-\tau_0\boldsymbol{e}_3\boldsymbol{e}_3^{\mathrm{T}} - 2\tau_2(\boldsymbol{e}_1\boldsymbol{e}_1^{\mathrm{T}} - \boldsymbol{e}_2\boldsymbol{e}_2^{\mathrm{T}})\right\}\\ &-\frac{15\mu}{r^5}\left\{-\boldsymbol{A}\left(\frac{\boldsymbol{I}}{m}\right)\boldsymbol{A}^{\mathrm{T}}\bar{\boldsymbol{r}}\bar{\boldsymbol{r}}^{\mathrm{T}} - \bar{\boldsymbol{r}}\bar{\boldsymbol{r}}^{\mathrm{T}}\boldsymbol{A}\left(\frac{\boldsymbol{I}}{m}\right)\boldsymbol{A}^{\mathrm{T}}\right.\\ &+\tau_0\bar{z}(\boldsymbol{e}_3\bar{\boldsymbol{r}}^{\mathrm{T}} + \bar{\boldsymbol{r}}\boldsymbol{e}_3^{\mathrm{T}})\\ &\left.+2\tau_2[\bar{x}(\boldsymbol{e}_1\bar{\boldsymbol{r}}^{\mathrm{T}} + \bar{\boldsymbol{r}}\boldsymbol{e}_1^{\mathrm{T}}) - \bar{y}(\boldsymbol{e}_2\bar{\boldsymbol{r}}^{\mathrm{T}} + \bar{\boldsymbol{r}}\boldsymbol{e}_2^{\mathrm{T}})]\right\}\end{aligned} \tag{19}$$

Because the system is conservative, there are only even terms in the characteristic polynomial of the system matrix $\boldsymbol{D}(\boldsymbol{r}_{\mathrm{e}})$, and the eigenvalues are symmetric with respect to both the real and imaginary axes. The eigenvector with a positive real eigenvalue is the unstable one, and the eigenvector with a negative real eigenvalue is the stable one. The normalized (to 1) stable and unstable eigenvectors are denoted as $\boldsymbol{Y}^{\mathrm{s}}(\boldsymbol{r}_{\mathrm{e}})$ and $\boldsymbol{Y}^{\mathrm{u}}(\boldsymbol{r}_{\mathrm{e}})$,

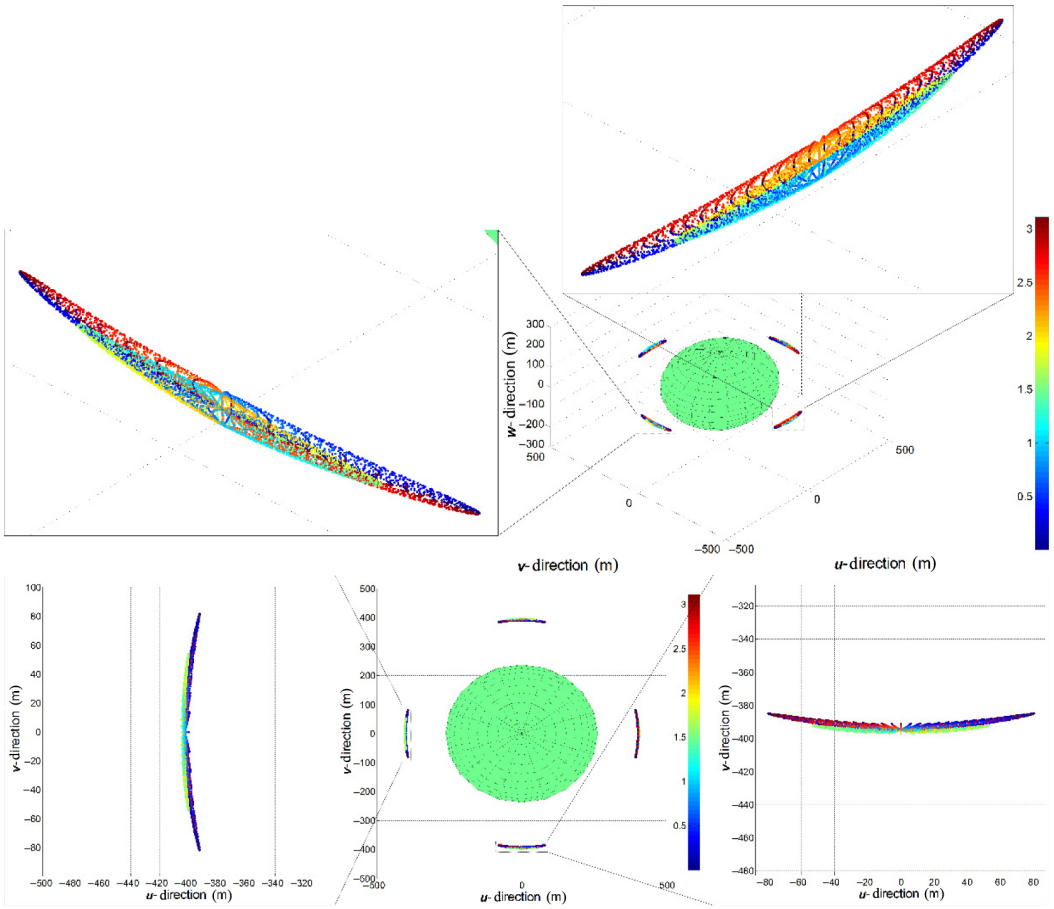

Fig. 9 Loci of out-of-plane equilibrium points with $\{\psi \in [0,\pi], \theta \in [0,\pi], \phi = 0\}$ and $\rho = 100$ m.

respectively. The stable and unstable vectors tangent to invariant manifolds can be obtained by perturbing the equilibrium point $\boldsymbol{r}_{\mathrm{e}}$ in the directions of $\boldsymbol{Y}^{\mathrm{s}}(\boldsymbol{r}_{\mathrm{e}})$ and $\boldsymbol{Y}^{\mathrm{u}}(\boldsymbol{r}_{\mathrm{e}})$, respectively:

$$\boldsymbol{X}^{\mathrm{s}}(\boldsymbol{r}_{\mathrm{e}}) = [\boldsymbol{r}_{\mathrm{e}}^{\mathrm{T}}, 0, 0, 0]^{\mathrm{T}} + \varepsilon \boldsymbol{Y}^{\mathrm{s}}(\boldsymbol{r}_{\mathrm{e}}) \tag{20}$$

$$\boldsymbol{X}^{\mathrm{u}}(\boldsymbol{r}_{\mathrm{e}}) = [\boldsymbol{r}_{\mathrm{e}}^{\mathrm{T}}, 0, 0, 0]^{\mathrm{T}} + \varepsilon \boldsymbol{Y}^{\mathrm{u}}(\boldsymbol{r}_{\mathrm{e}}) \tag{21}$$

where ε represents a small displacement from $\boldsymbol{r}_{\mathrm{e}}$.

The stable and unstable manifolds can be obtained by integrating the stable vector $\boldsymbol{X}^{\mathrm{s}}(\boldsymbol{r}_{\mathrm{e}})$ backwards and the unstable vector $\boldsymbol{X}^{\mathrm{u}}(\boldsymbol{r}_{\mathrm{e}})$ forwards, respectively. As a demonstration, we calculate the stable and unstable manifolds for some of the out-of-plane equilibrium points with $\{\psi \in [0,\pi], \theta = 0, \phi \in [0,\pi]\}$ and $\rho = 100$ m given in Section 4.2. The out-of-plane equilibrium points are distributed in four regions consisting of closed curves. The equilibrium-point groups near the $\boldsymbol{v}$-axis all have three pairs of imaginary eigenvalues, and there are no stable or unstable manifolds for these points. The equilibrium-point groups near the $\boldsymbol{u}$-axis all have two pairs of imaginary eigenvalues and a pair of real eigenvalues, indicating that the stable and unstable manifolds exist. Because the loci and stability of equilibrium points are symmetric with respect to the center of the asteroid, only the stable and unstable manifolds associated with equilibrium points near the $-\boldsymbol{u}$-axis are calculated here.

The loci of the out-of-plane equilibrium points of the group near the $-\boldsymbol{u}$-axis with $\{\psi \in [0,\pi], \theta = 0, \phi \in [0,\pi]\}$ form a 2D surface consisting of infinitely many closed curves, each of which is formed by out-of-plane equilibrium points with $\{\psi = \psi_{\mathrm{curve}}, \theta = 0, \phi \in [0,\pi]\}$. The stable and unstable manifolds associated with the closed curves formed by the out-of-plane equilibrium points with $\left\{\psi = \frac{\pi}{4}, \theta = 0, \phi \in [0,\pi]\right\}$ and $\left\{\psi = \frac{3\pi}{4}, \theta = 0, \phi \in [0,\pi]\right\}$ are shown in Figs. 11 and 12, respectively. The equilibrium points with manifolds plotted in Fig. 11 are marked by black stars, and other out-of-plane equilibrium points are marked by black dots. The stable and unstable manifolds are shown in blue and red, respectively.

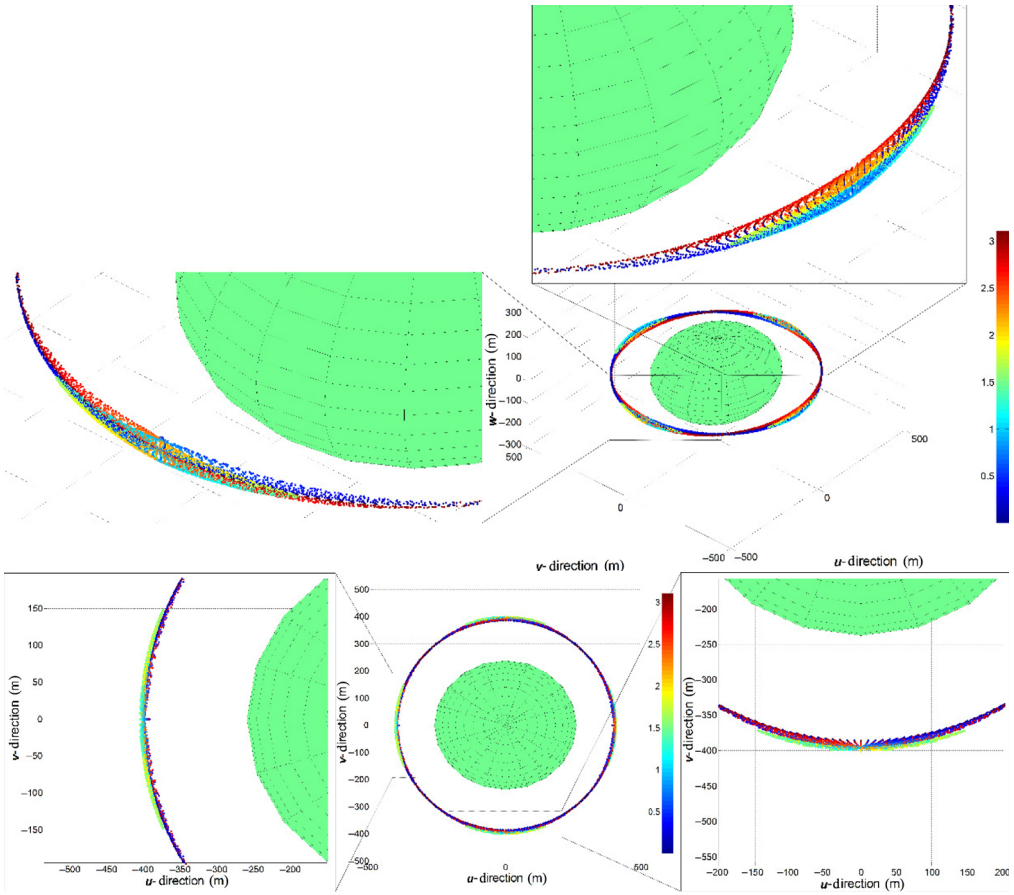

Fig. 10 Loci of out-of-plane equilibrium points with $\{\psi \in [0, \pi], \theta \in [0, \pi], \phi = 0\}$ and $\rho = 160$ m.

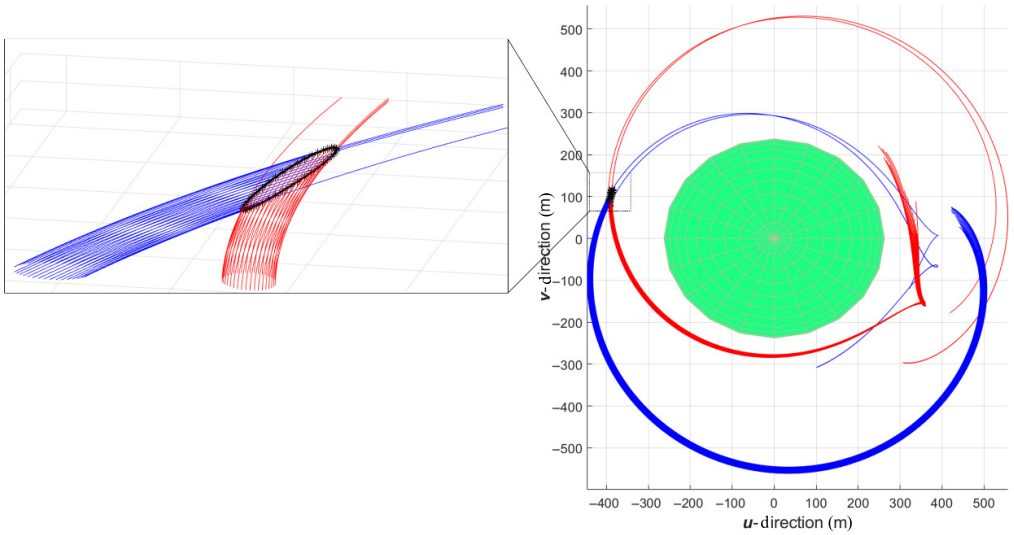

Fig. 11 Stable and unstable manifolds associated with out-of-plane equilibrium points with $\left\{\psi = \frac{\pi}{4}, \theta = 0, \phi \in [0, \pi]\right\}$.

For both cases, the stable and unstable manifolds are similar to the manifolds associated with periodic orbits. When the angle ϕ is close to 0 or $\pi/2$, the directions of the manifolds are opposite those for other values of ϕ. Another phenomenon is that most of the stable manifolds associated with out-of-plane equilibrium points with $\left\{\psi = \frac{\pi}{4}, \theta = 0, \phi \in [0, \pi]\right\}$ move away from the asteroid, whereas most of the stable manifolds

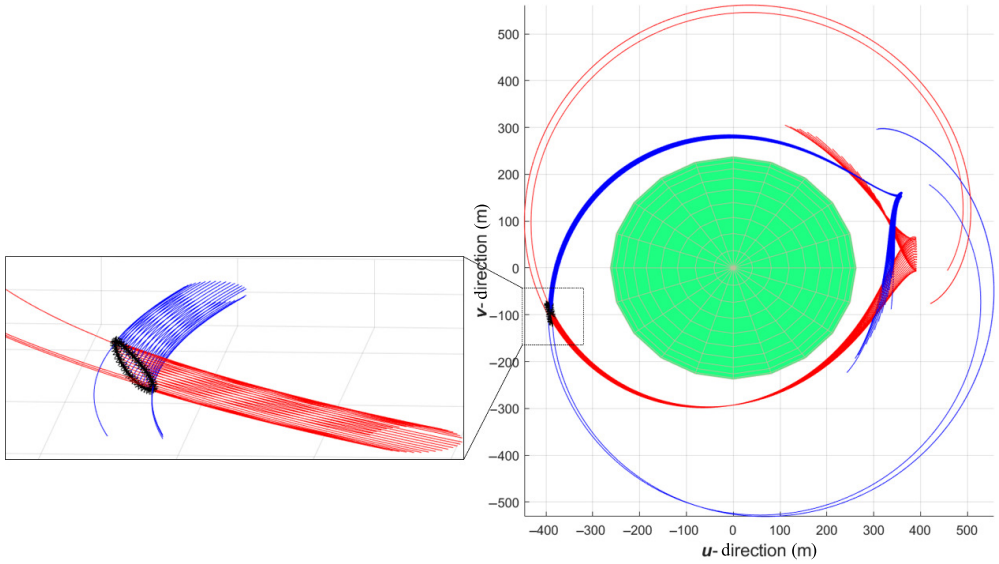

Fig. 12 Stable and unstable manifolds associated with out-of-plane equilibrium points with $\{\psi = \frac{3\pi}{4}, \theta = 0, \phi \in [0, \pi]\}$.

associated with out-of-plane equilibrium points with $\{\psi = \frac{3\pi}{4}, \theta = 0, \phi \in [0, \pi]\}$ approach the asteroid.

The stable and unstable manifolds associated with the out-of-plane equilibrium points with $\{\psi = [0, \pi], \theta = 0, \phi \in [0, \pi]\}$ are shown in Fig. 13. Most of the stable manifolds associated with the out-of-plane equilibrium points with $\{\psi \in [0, \frac{\pi}{2}), \theta = 0, \phi \in [0, \pi]\}$ move away from the asteroid, whereas most of the stable manifolds

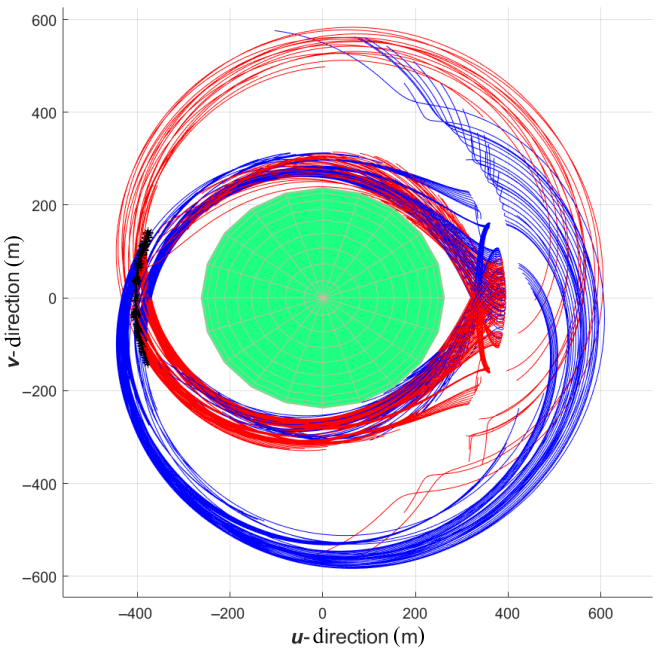

Fig. 13 Stable and unstable manifolds associated with the out-of-plane equilibrium points with $\{\psi = [0, \pi], \theta = 0, \phi \in [0, \pi]\}$.

associated with out-of-plane equilibrium points with $\{\psi \in (\frac{\pi}{2}, \pi], \theta = 0, \phi \in [0, \pi]\}$ approach the asteroid.

These results indicate that in addition to the locations of the equilibrium points, the attitude of the spacecraft significantly affects the invariant manifolds of equilibrium points, and it can provide more options for trajectory design in close proximity to asteroids.

6 Conclusions

Out-of-plane equilibrium points of the attitude-restricted orbital dynamics about an asteroid, which are outside the principal planes of the asteroid, were investigated via numerical calculations and subsequent analyses. The attitude-restricted orbital dynamics in proximity to asteroids were recently proposed, where the GOACP is taken into account, in addition to the non-spherical gravity of the asteroid.

According to the general equilibrium condition containing all the three Euler angles, out-of-plane equilibrium points were calculated via iterations by using the equatorial equilibrium points with nonzero Euler angle ψ as starting points. Two simplified cases were considered: equilibrium points with $\{\psi \in [0, \pi], \theta = 0, \phi \in [0, \pi]\}$ and $\{\psi \in [0, \pi], \theta \in [0, \pi], \phi = 0\}$. The results indicated that the loci of out-of-plane equilibrium points with two nonzero Euler angles form 2D surfaces consisting of infinitely many closed curves, which are obtained by changing the Euler angle ϕ or θ gradually. The 2D surface can be parameterized by the pair of Euler angles

$\{\psi, \phi\}$ or $\{\psi, \theta\}$. The 2D surface surrounds the in-plane equatorial equilibrium points, which can be regarded as its framework. For a small characteristic dimension, the 2D surface is distributed near the equatorial axes of the asteroid, whereas for a large characteristic dimension, the 2D surface can be distributed at any longitude of the asteroid owing to the significant GOACP.

The invariant manifolds associated with out-of-plane equilibrium points with $\{\psi \in [0, \pi], \theta = 0, \phi \in [0, \pi]\}$ and $\rho = 100$ m were calculated as a demonstration. Owing to the symmetry of the equilibrium points, only the stable and unstable manifolds associated with equilibrium points near the $-\boldsymbol{u}$-axis were examined in this study. The stable and unstable manifolds associated with the closed curve formed by out-of-plane equilibrium points with $\{\psi = \psi_{\text{curve}}, \theta = 0, \phi \in [0, \pi]\}$ form tubes, but the directions of these manifolds are opposite those of others when the Euler angle ϕ is close to 0 or $\pi/2$. The Euler angle ψ also affects the invariant manifolds. Most of the stable manifolds move away from the asteroid with $\psi \in \left[0, \frac{\pi}{2}\right)$, and most of the stable manifolds approach the asteroid with $\psi \in \left(\frac{\pi}{2}, \pi\right]$.

Although out-of-plane equilibrium points with three nonzero Euler angles were not calculated in this study, it can be expected that the loci of out-of-plane equilibrium points with $\{\psi \in [0, \pi], \theta \in [0, \pi], \phi \in [0, \pi]\}$ form a 3D geometric object consisting of infinitely many 2D surfaces, which are formed by the loci of out-of-plane equilibrium points with two nonzero Euler angles. The 3D geometric object can be parameterized by the three Euler angles $\{\psi, \theta, \phi\}$.

Acknowledgements

This work was supported by the National Natural Science Foundation of China under Grant Nos. 11602009, 11432001 and 11872007, as well as the Fundamental Research Funds for the Central Universities.

Declaration of competing interest

The authors have no competing interests to declare that are relevant to the content of this article.

References

[1] Wang, Y., Xu, S. J. Orbital dynamics and equilibrium points around an asteroid with gravitational orbit–attitude coupling perturbation. *Celestial Mechanics and Dynamical Astronomy*, **2016**, 125(3): 265–285.

[2] Wang, Y., Xu, S. J. Non-equatorial equilibrium points around an asteroid with gravitational orbit-attitude coupling perturbation. *Astrodynamics*, **2020**, 4(1): 1–16.

[3] Russell, R. P. Survey of spacecraft trajectory design in strongly perturbed environments. *Journal of Guidance, Control, and Dynamics*, **2012**, 35(3), 705–720.

[4] Scheeres, D. J. Orbit mechanics about asteroids and comets. *Journal of Guidance, Control, and Dynamics*, **2012**, 35(3): 987–997.

[5] Scheeres, D. J. Orbit mechanics about small bodies. *Acta Astronautica*, **2012**, 72: 1–14.

[6] Scheeres, D. J. *Orbital Motion in Strongly Perturbed Environments*. Springer, Berlin, Heidelberg, **2012**.

[7] Scheeres, D. J. Close proximity dynamics and control about asteroids. In: Proceedings of the 2014 American Control Conference, **2014**: 1584–1598.

[8] Riverin, J. L., Misra, A. K. Attitude dynamics of satellites orbiting small bodies. In: Proceedings of the AIAA/AAS Astrodynamics Specialist Conference and Exhibit, **2002**: AIAA 2002-4520.

[9] Misra, A. K., Panchenko, Y. Attitude dynamics of satellites orbiting an asteroid. *The Journal of the Astronautical Sciences*, **2006**, 54(3–4): 369–381.

[10] Kumar, K. D. Attitude dynamics and control of satellites orbiting rotating asteroids. *Acta Mechanica*, **2008**, 198(1–2): 99–118.

[11] Wang, Y., Xu, S. J. Attitude stability of a spacecraft on a stationary orbit around an asteroid subjected to gravity gradient torque. *Celestial Mechanics and Dynamical Astronomy*, **2013**, 115(4): 333–352.

[12] Wang, Y., Xu, S. Equilibrium attitude and nonlinear stability of a spacecraft on a stationary orbit around an asteroid. *Advances in Space Research*, **2013**, 52(8): 1497–1510.

[13] Wang, Y., Xu, S. Analysis of the attitude dynamics of a spacecraft on a stationary orbit around an asteroid via Poincaré section. *Aerospace Science and Technology*, **2014**, 39: 538–545.

[14] Zhang, M. J., Zhao, C. Y. Attitude stability of a spacecraft with two flexible solar arrays on a stationary orbit around an asteroid subjected to gravity gradient torque. *Astrophysics and Space Science*, **2014**, 351(2): 507–524.

[15] Zhang, M. J., Zhao, C. Y. Attitude stability of a dual-spin spacecraft on a stationary orbit around an asteroid subjected to gravity gradient torque. *Astrophysics and Space Science*, **2015**, 355(2): 203–212.

[16] Scheeres, D. J. Spacecraft at small NEO. **2006**: arXiv: physics/0608158v1. Available at https://arxiv.org/abs/physics/0608158.

[17] Wang, Y., Xu, S. Gravitational orbit-rotation coupling

of a rigid satellite around a spheroid planet. *Journal of Aerospace Engineering*, **2014**, 27(1): 140–150.

[18] Sincarsin, G. B., Hughes, P. C. Gravitational orbit-attitude coupling for very large spacecraft. *Celestial Mechanics*, **1983**, 31(2): 143–161.

[19] Wang, L. S., Krishnaprasad, P. S., Maddocks, J. H. Hamiltonian dynamics of a rigid body in a central gravitational field. *Celestial Mechanics and Dynamical Astronomy*, **1990**, 50(4): 349–386.

[20] Wang, L.-S., Maddocks, J. H., Krishnaprasad, P. S. Steady rigid-body motions in a central gravitational field. *Journal of Astronautical Sciences*, **1992**, 40: 449–478.

[21] Sanyal, A. K. Dynamics and control of multibody systems in central gravity. Ph.D. Dissertation. Ann Harbor, MI: Department of Aerospace Engineering, The University of Michigan, **2004**.

[22] Teixidó Román, M. Hamiltonian methods in stability and bifurcations problems for artificial satellite dynamics. Master Thesis. Facultat de Matemàtiques i Estadística, Universitat Politècnica de Catalunya, **2010**: 51–72.

[23] Wang, Y., Xu, S. Symmetry, reduction and relative equilibria of a rigid body in the J_2 problem. *Advances in Space Research*, **2013**, 51(7): 1096–1109.

[24] Wang, Y., Xu, S. J. Stability of the classical type of relative equilibria of a rigid body in the J_2 problem. *Astrophysics and Space Science*, **2013**, 346(2): 443–461.

[25] Wang, Y., Xu, S. J. Relative equilibria of full dynamics of a rigid body with gravitational orbit-attitude coupling in a uniformly rotating second degree and order gravity field. *Astrophysics and Space Science*, **2014**, 354(2): 339–353.

[26] Wang, Y., Xu, S. J., Tang, L. On the existence of the relative equilibria of a rigid body in the J_2 problem. *Astrophysics and Space Science*, **2014**, 353(2): 425–440.

[27] Wang, Y., Xu, S. J. On the nonlinear stability of relative equilibria of the full spacecraft dynamics around an asteroid. *Nonlinear Dynamics*, **2014**, 78(1): 1–13.

[28] Hu, W., Yin, T., Zheng, W., Deng, Z. Symplectic analysis on orbit-attitude coupling dynamic problem of spatial rigid rod. *Journal of Vibration and Control*, **2020**, 26(17–18): 1614–1624.

[29] Kikuchi, S., Howell, K. C., Tsuda, Y., Kawaguchi, J. Orbit-attitude coupled motion around small bodies: Sun-synchronous orbits with Sun-tracking attitude motion, *Acta Astronautica*, **2017**, 140: 34–48.

[30] Jean, I., Misra, A. K., Ng, A. Orbital and attitude coupled dynamics of a spacecraft around an asteroid. In: Proceedings of the 3rd IAA Conference on Dynamics and Control of Space Systems, **2017**.

[31] Lee, D., Sanyal, A. K., Butcher, E. A., Scheeres, D. J. Almost global asymptotic tracking control for spacecraft body-fixed hovering over an asteroid. *Aerospace Science and Technology*, **2014**, 38: 105–115.

[32] Lee, D., Sanyal, A. K., Butcher, E. A., Scheeres, D. J. Finite-time control for spacecraft body-fixed hovering over an asteroid. *IEEE Transactions on Aerospace and Electronic Systems*, **2015**, 51(1): 506–520.

[33] Misra, G., Izadi, M., Sanyal, A., Scheeres, D. J. Coupled orbit–attitude dynamics and pose estimation of spacecraft near small solar system bodies. *Advances in Space Research*, **2016**, 57(8), 1747–1761 .

[34] Li, X., Warier, R. R., Sanyal, A. K., Qiao, D. Trajectory tracking near small bodies using only attitude control. *Journal of Guidance, Control, and Dynamics*, **2019**, 42(1): 109–122.

[35] Hu, W., Yu, L., Deng, Z. Minimum control energy of spatial beam with assumed attitude adjustment target. *Acta Mechanica Solida Sinica*, **2020**, 33: 51–60.

[36] Howard, J. E. Spectral stability of relative equilibria. *Celestial Mechanics and Dynamical Astronomy*, **1990**, 48(3): 267–288.

Yue Wang received his B.Eng. and Ph.D. degrees in aerospace engineering from Beihang University (formerly known as Beijing University of Aeronautics and Astronautics), Beijing, China, in 2009 and 2014, respectively. From 2014 to 2015, he worked as a postdoctoral fellow in the Distributed Space Systems Lab in the Faculty of Aerospace Engineering at Technion–Israel Institute of Technology, Haifa, Israel. In 2016, he joined the School of Astronautics at Beihang University as an associate professor of the "Zhuoyue" Recruitment Program. He was rewarded the Young Elite Scientist Sponsorship Program by China Association for Science and Technology. His current research interests center on orbital dynamics and control about asteroids and the Earth–Moon system, orbital evolution and reentry prediction of space debris, and NEO impact hazard assessment. E-mail: ywang@buaa.edu.cn.

Ruikang Zhang received his B.Eng. degree in aerospace engineering from Beihang University (formerly known as Beijing University of Aeronautics and Astronautics), Beijing, China, in 2017. At present, he is a Ph.D. candidate in aerospace engineering at Beihang University. His research interests include orbital dynamics and control about asteroids and the Earth–Moon system. E-mail: zhangruikang@buaa.edu.cn.